DESIGN AND TESTING OF A WINGED SUBSOILER SHOVEL FOR STRIP MINIMUM-TILLAGE DEEP LOOSENING FERTILISER MACHINE
/
条带少耕深松施肥机带翼式深松铲设计与试验

Shi-cheng XU [1]; Gui-xiang TAO *[1]; Shu-juan YI [1]; Song WANG [1]; Yu-hang SAN [1]
College of Engineering, Heilongjiang Bayi Agricultural University, Daqing/P. R. China
Tel: +86-459-13836961877; E-mile: 15628820228@163.COM;
Corresponding author: Gui-xiang TAO
DOI: https://doi.org/10.35633/inmateh-76-78

Keywords: *strip minimum tillage; subsoiling fertilizer applicators; winged subsoiler shovels; discrete element method*

ABSTRACT
To address issues such as soil compaction, plough layer damage, and hardpan formation caused by long-term use of rotary tillage and conventional ploughing, a winged subsoiler shovel was designed based on the soil characteristics of the black soil region in Northeast China. A mechanical contact model between the subsoiler shovel and soil was established to identify the design factors affecting the operational quality of the shovel. Using discrete element simulation technology, a shovel-soil interaction model was constructed. Through a quadratic regression rotational orthogonal design test, the effects of shovel structural parameters on soil disturbance area were determined. Taking the maximization of soil disturbance area as the objective, the shovel parameters were optimized. The optimal parameter combination was obtained as follows: shovel tip entry angle of 21°, wing inclination angle of 28°, and wing width of 104 mm, resulting in a maximum soil disturbance area of 1699.80 cm². A bench verification test was subsequently conducted, showing an actual soil disturbance area of 1666.08 cm². The test results were consistent with the simulation optimization results, confirming that the optimal parameter combination meets operational requirements and satisfies agronomic needs for deep loosening.

摘要
针对于长期使用旋耕、翻耕等耕整地方式造成土壤板结、犁地层破坏、犁底层板结等问题，基于中国东北黑土区土壤特性设计了一种带翼式深松铲。建立了深松铲与土壤间的力学接触模型，确定了影响深松铲作业质量的深松铲设计因素。应用离散元仿真技术，建立了深松铲-土壤仿真模型，通过二次回归旋转正交组合试验，确定了深松铲结构参数对土壤扰动面积的影响规律，以土壤扰动面积最大化为目标，对深松铲参数进行优化求解，深松铲的最优参数组合为：铲尖入地角为 21°、铲翼倾角为 28°、铲翼宽度为 104mm 时，土壤扰动面积最大，土壤扰动面积为 1699.80cm²。得出最优参数后进行台架验证试验，台架试验结果表明：实际土壤扰动面积为 1666.08cm²，试验结果与仿真优化结果基本一致，最优参数组合符合作业要求，满足深松农艺要求。

INTRODUCTION
Since the 1980s, the mode of ploughing operation has been transitioning from the full-tillage operation with a large amount of soil movement to the no-tillage operation mode such as less-tillage and no-tillage (*Zhang et al., 2024*). Among them, less tillage provides a certain degree of soil disturbance, which can improve soil aeration, effectively prevent soil sloughing, and improve the degree of plough subsoil sloughing and damage (*Wang et al., 2021*). Strip minimum tillage is mainly to return the straw to the rows, so that the surface of the ground to form a strip to be sown (*Gao et al., 2023*). During strip minimum tillage, the subsoiler shovel further optimizes the soil tillage structure. Subsoiling loosens the soil along predetermined strips, increasing the depth and range of soil loosening, which can better break up the plough pan, promote deep root growth of crops, and thereby increase crop yields.

[1] *Shi-cheng Xu, M.S.; Gui-xiang Tao, Prof. Ph.D.; Shu-juan Yi, Prof. Ph.D.; Song Wang, Ph.D.; Yu-hang San, Ms.*

At present, limited research has been conducted on the winged subsoiler shovel used in strip minimum-tillage deep loosening fertilizer machines *(Zhao et al., 2018)*. Most related studies focus on the structural design and optimization of subsoiler shovels used in ploughing components, with particular emphasis on the structural design of the shovel itself. *Zheng et al., (2016*), designed a subsoiler shovel with a folded breaking edge for effective drag reduction and consumption reduction through discrete element simulation and field tests. *Manuwa, (2009),* investigated the effects of different subsoiler shovel tip designs and entry angles on soil disturbance. *Li et al., (2018),* conducted a comparative analysis of two types of subsoiler shovels, with and without wings. The results showed that winged subsoiler shovels exhibited better performance in terms of ploughing resistance and soil disturbance compared with non-winged shovels. Specifically, the tillage resistance and disturbed area of winged subsoiler shovels were more than twice those of non-winged shovels. However, existing research has not yet integrated the strip minimum tillage mode to develop specialized subsoiler shovels, and conventional designs demonstrate poor adaptability, thereby reducing the quality of machine operation.

Based on the soil characteristics of the black soil region in Northeast China, this study designs a subsoiler shovel adapted to the strip minimum tillage mode. Discrete element method (DEM) simulation was used to optimize the structural parameters of the subsoiler shovel, aiming to develop a winged design that maximizes soil disturbance. The optimal parameters were verified through bench testing, confirming the effectiveness of the proposed winged subsoiler shovel.

MATERIALS AND METHODS

Structure and working principle

The strip minimum-tillage deep loosening fertilizing machine consists of a straw-clearing and cutting mechanism and a subsoiling mechanism. The winged subsoiler shovel is composed of a shovel tip, shovel handle, and shovel wings, and is mounted onto the subsoiling mechanism after the straw-clearing and cutting unit. The subsoiling mechanism is connected to the rear of the straw-clearing and cutting mechanism via a connecting frame. The subsoiler shovel is fixed to the mounting handle, which is in turn secured to the connecting frame of the subsoiling mechanism using bolts. The working depth of the subsoiler shovel can be adjusted by selecting different mounting holes on the handle, allowing adaptation to various agronomic requirements. The structural design of the strip minimum-tillage fertilizing machine and the winged subsoiler shovel is illustrated in Fig. 1.

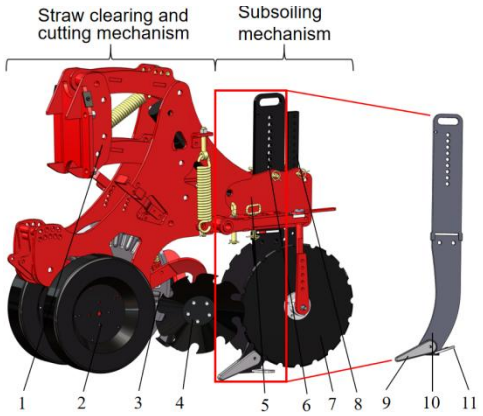

Fig. 1 – Structure of the strip minimum-tillage deep loosening fertilizing machine and winged subsoiler shovel

1. Four-link connecting bracket; 2. Depth-limiting wheel; 3. Stubble-cutting disc knife; 4. Notched straw-clearing disc; 5. Subsoiling mechanism connecting frame; 6. Subsoiler shovel; 7. Disc harrow; 8. Fertilizer tube; 9. Shovel tip; 10. Shovel handle; 11. Shovel wings

When the subsoiler shovel carries out deep loosening operation, under the action of traction force, the subsoiler shovel cuts into the soil at a certain angle and moves forward, continuously squeezes the soil in front of it, and produces a continuous shear force on the soil, and under the action of the shear force, the soil gradually breaks up and loosens, and pushes the soil to the two sides to form a loose ridge, thus arriving at the effect of soil loosening. At the same time, the side and bottom of the subsoiler shovel will also produce extrusion and friction on the soil, which can further break the soil. The cutting and crushing action of the subsoiler shovel on the soil can make the soil particles rearrange, increase the soil porosity and improve the soil structure.

Mechanical analysis of the subsoiling process

To investigate the forces acting on the subsoiler shovel during the subsoiling process, a mechanical analysis of the shovel tip is conducted, and a mechanical contact model between the shovel tip and the soil is established, as shown in Fig. 2(a). The shovel tip of the subsoiler is simplified as an inclined plane subjected to force. When this inclined plane is pushed forward horizontally in the soil, shear failure occurs on the soil surface in front of the shovel tip as well as in the soil above it (*Zhang, 2013*).

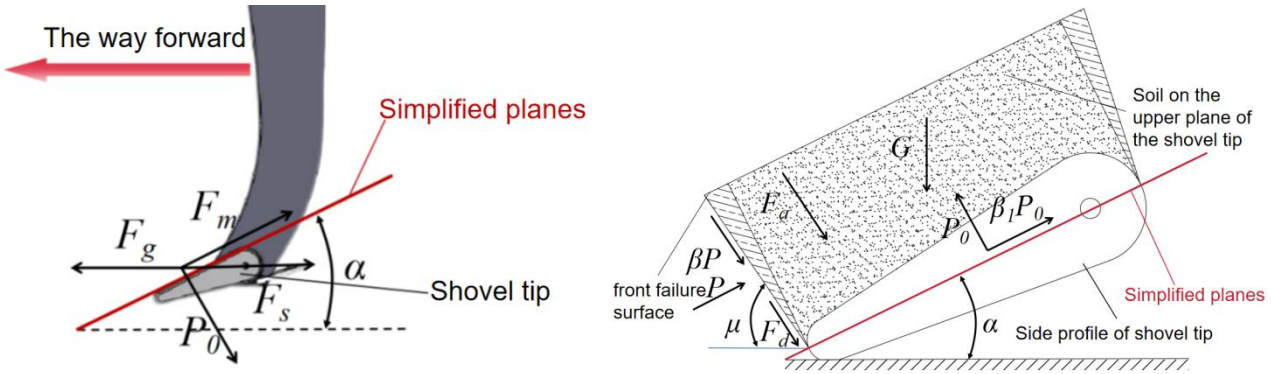

(a) Analysis of forces in subsoiler shovel tip operation (b) Analysis of soil forces in the upper plane of the shovel tip

Fig. 2 – Force analysis diagram of shovel tip

According to Fig. 2(a), the equilibrium equation of force on shovel tip can be obtained:

$$\begin{aligned} F_q &= P_0 \sin\alpha + F_m \cos\alpha + F_s \\ F_m &= P_0\beta \end{aligned} \quad (1)$$

where: F_q is the traction force, N; P_0 is the normal load of the soil on the shovel tip, N; α is the angle of shovel tip into the ground, (°); F_m is the friction of the soil on the upper plane of the shovel tip, N; F_s is the cutting resistance of the soil on the shovel tip, N; and β_1 is the friction factor between the soil and the shovel tip.

The soil cutting resistance is negligible due to the fact that there are fewer hard stones and other hard debris in normal ploughed soils during subsoiling, and the cutting resistance of the soil is small (*Ma, 2022*). Therefore, from Equation (1), it can be seen that the traction force is related to the normal load of the soil on the shovel tip, the friction factor between the soil and the shovel tip, and the shovel tip entry angle. The traction force and the horizontal ploughing resistance of shovel tip are equilibrium forces, so the horizontal ploughing resistance is related to the normal load of soil on the shovel tip, the friction factor between soil and shovel tip, and the angle of shovel tip into the ground.

In order to deeply investigate the influence mechanism of the structural parameters of the shovel tip on the effect of subsoiler shovelling operation, it is necessary to carry out a mechanical analysis of the soil on the plane of the shovel tip, as shown in Fig. 2 (b).

According to Fig. 2 (b) and Eq. (1), the equilibrium equation for the force on the plane soil on the shovel tip can be obtained:

$$F_q = P(\sin\mu + \beta\cos\mu) + (F_d + F_a)\cos\mu \quad (2)$$

$$F_q\left(\frac{\cos\alpha - \beta_1\sin\alpha}{\sin\alpha + \cos\alpha} + \frac{\cos\mu - \beta\sin\mu}{\sin\mu + \beta\cos\mu}\right) = G + (F_d + F_a)\sin\mu + (F_d - F_a)\sin\mu\frac{\cos\mu - \beta\sin\mu}{\sin\mu + \beta\cos\mu} \quad (3)$$

where: P is the normal load of the soil front failure surface on the shovel tip, N; μ is the inclination angle of the soil front failure surface on the shovel tip, (°); β is the internal friction factor of the soil; F_d is the cohesion force of the soil, N; F_a is the acceleration force of the soil, N; G is the gravity force of the soil on the shovel tip, N.

Where the soil gravity in the plane on the shovel tip in equation (3) can be calculated from the volume of soil supported by the shovel tip (*Zhou, 2006*), the soil gravity is calculated as:

$$G = \rho g C_k H\left(\frac{\sin(\alpha+\mu)}{\sin\mu}\right)\left\{C_l + H\frac{[\cos(\alpha+\mu) + \tan\alpha\sin(\alpha+\mu)]}{2\sin\mu}\right\} \quad (4)$$

where: ρ is the soil density, kg/m^3; H is the depth of subsoiler shovelling, mm; C_k is the width of shovel tip, mm; C_l is the length of shovel tip, mm.

Based on the formula for soil cohesion, a theoretical expression for soil cohesion can be derived:

$$F_d = d\frac{HL}{\sin\mu} \quad (5)$$

where:

d is the soil cohesion per unit of shear failure surface, Pa;

L is the arc length of the front plane of the shovel tip, mm.

Based on the theoretical derivation of the soil acceleration force by Newton's second law, the cutting failure process of the Subsoiling shovel on the soil during ploughing can be regarded as a quasi-static continuous motion process, so the acceleration force on the soil can be characterized as a steady state acceleration force, and its magnitude can be calculated by the mass of the accelerated soil per unit of time, and the calculation formula:

$$F_a = \rho C_k HVV_1 \quad (6)$$

where: V is the speed of subsoiler shovel, m/s; V_1 is the instantaneous speed of subsoiler shovel tip, m/s.

The equilibrium equation was derived by substituting Equations (4), (5), and (6) into Equation (3):

$$F_q = P(\sin\mu + \beta\cos\mu) + \left(d\frac{HL}{\sin\mu} + \rho C_K HVV_1\right)\cos\mu \quad (7)$$

$$F_q\left(\frac{\cos\alpha - \beta_1\sin\alpha}{\sin\alpha + \cos\alpha} + \frac{\cos\mu - \beta\sin\mu}{\sin\mu + \beta\mu}\right) = \rho g C_k H\left(\frac{\sin(\alpha+\mu)}{\sin\mu}\right)\left\{C_l + H\frac{[\cos(\alpha+\mu) + \tan\alpha\sin(\alpha+\mu)]}{2\sin\mu}\right\}$$

$$+\left[d\frac{HL}{\sin\mu} + \rho C_K HVV_1\right]\sin\mu + \left[d\frac{HL}{\sin\mu} - \rho C_K HVV_1\right]\sin\mu\frac{\cos\mu - \beta\sin\mu}{\sin\mu + \beta\cos\mu} \quad (8)$$

Based on the shear failure theory in soil mechanics, the angle of inclination of the front failure surface of the soil on the upper plane of the shovel tip can be studied and derived, resulting in a theoretical expression for the angle of inclination of the front failure surface of the soil.

The expression is:

$$\mu = \frac{\pi}{2} - \arctan\frac{\varpi}{2} \quad (9)$$

where: ϖ is the angle of internal friction of the soil, (°).

Based on the analysis of the mechanical contact model, the soil disturbance range of the shovel tip and the tillage resistance can be determined by soil mechanical parameters (e.g., cohesion, internal friction angle, density), tillage condition parameters (e.g., tillage depth, tillage speed), and geometric parameters of the shovel tip (e.g., entry angle, width, and length). Since soil mechanical properties are generally uncontrollable during the design process, the influence of the shovel tip on soil disturbance primarily depends on its geometric parameters, particularly key variables such as the entry angle, width, and length. According to *Zhou (2006)*, among these parameters, the soil entry angle exerts the most significant influence on the performance of the subsoiler shovel. Selecting an appropriate entry angle can effectively reduce ploughing resistance and enhance soil disturbance. In contrast, the width and length of the shovel tip have relatively smaller effects, mainly influencing the uniformity of soil fragmentation and the stability of ploughing.

The shovel handle exerts a cutting effect on the soil primarily through frictional resistance and contact resistance. For the force analysis, soil particles along the curve of the shovel handle were treated as mass points. The mechanical contact model between the soil and the shovel handle is illustrated in Fig. 3(a).

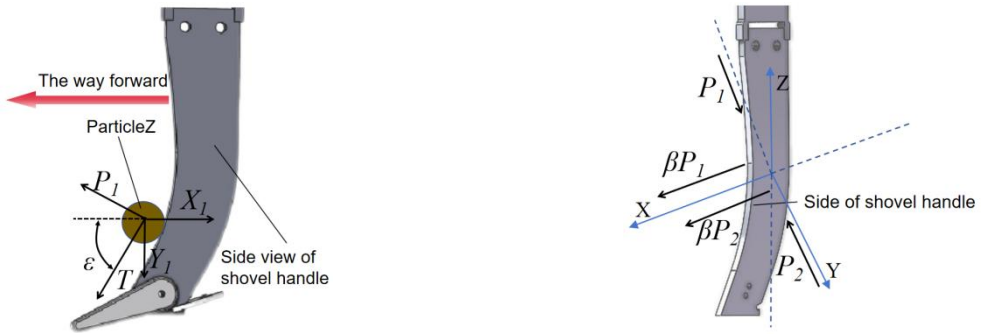

(a) Analysis of forces on soil mass points of shovel handle (b) Shovel handle side force analysis

Fig. 3 – Force analysis of shovel handle

Assuming the soil is homogeneous, the interaction force between soil particles follows Coulomb's law. According to Coulomb's friction law, the frictional force and normal pressure between soil particles are proportional. Thus, the relationship between the normal pressure and tangential force at the soil particle mass point can be expressed as:

$$T = F_d + P_1 \tan \varpi \quad (10)$$

where: T is the tangential force of the shovel handle on the soil particle mass point, N; P_1 is the positive pressure of the curved shovel handle on the soil particle mass point, N.

According to Fig. 3 (a) as well as Eq. (10), the equilibrium equations of force on the soil mass are obtained:

$$X_1 = \left(P_1 + F_d + P_1 \tan \varpi\right)\cos \varepsilon \quad (11)$$

$$Y_1 = (P_1 - F_d - P_1 \tan \varpi)\sin \varepsilon \quad (12)$$

where: X_1 is the horizontal force of the resistance given by the soil particles around the soil particle mass point, N; P_1 is the positive pressure of the curved shovel handle on the soil particle mass point, N; Y_1 is the vertical force of the resistance given by the soil particles around the soil particle mass point, N; ε is the angle of tangency between the soil particle mass point and the shovel handle, (°).

According to Equations (11) and (12), the force acting on soil particle mass point Z consists of the tangential component, determined by the push tangent angle (ε) between the soil particle and the shovel handle, and the resistance exerted by the surrounding soil particles in the vertical direction. As the soil particle mass point moves along the shovel handle, the push tangent angle reaches its maximum when the particle is at the vertical position, at which point Y_1 is maximized and X_1 minimized. Owing to the principle of action and reaction, the force exerted on the soil particle by the shovel handle generates an equal and opposite reaction force from the soil particle onto the shovel handle.

To further examine the influence of shovel handle side width on tillage resistance, the forces acting on both sides of the shovel handle were analysed. The side-force diagram of the shovel handle is presented in Fig. 3(b). Based on Fig. 3(b), the equilibrium equation for the forces on the shovel handle side can be derived as follows:

$$F_c = \beta P_1 + \beta P_2 \quad (13)$$

where:

F_c is the shovel handle side friction resistance, N; P_1, P_2 is the soil on the shovel handle side normal load, N.

The shovel handle is a symmetrical structure with equal areas on both sides, so the pressure on both sides is equal.

$$P_1 = P_2 = S_1 U$$
$$F_c = 2\beta\, S_1 U \quad (14)$$

where:

S_1 is the side area of shovel handle, mm^2; U is the coefficient of friction between soil and side of shovel handle.

The frictional resistance on both sides of the subsoiler shovel handle, as described by Equation (14), is influenced by the side surface area. Therefore, the side area should not be excessively large, as it would increase tillage resistance. However, according to the analysis based on Equations (11) and (12), the shovel handle is prone to stress concentration. Additionally, it is subjected to alternating bending loads and torsional loads caused by soil resistance eccentricity. If the side area is too small, the structural load-bearing capacity of the shovel handle is reduced, increasing the risk of mechanical failure. Thus, an appropriate balance must be maintained to optimize both resistance and structural integrity.

In the force analysis of the shovel wings, they are simplified as an inclined plane, with force conditions analogous to those of the shovel tip. Therefore, the parameters influencing the performance of the shovel wings can be referenced from those of the shovel tip.

Subsoiler shovel design

The chisel-type shovel tip penetrates the soil more effectively, with reduced extrusion of the surrounding soil. This allows it to quickly break through the plough pan while ensuring uniform lateral movement of the soil, thereby achieving more consistent loosening and enhancing the subsoiling effect. Given the high soil density and compact plough pan in the black soil region of Northeast China, a chisel-type shovel tip was selected. According to the JB/T9788–2020 standard "*Subsoiler Shovel and Subsoiler Shovel Handle"*, the shovel tip length and width were set at 165 mm and 40 mm, respectively. The structure of the shovel tip is illustrated in Fig. 4(a).

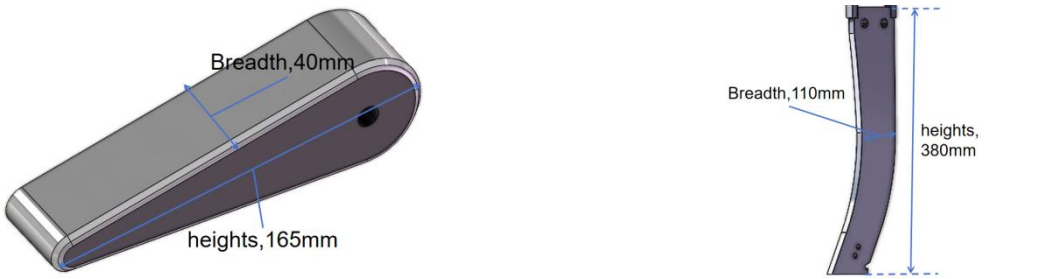

(a) Shovel tip structure drawing (b) Shovel handle structure drawing

Fig. 4 – Structure of shovel tip and shovel handle

According to the mechanical contact model between the soil and the shovel tip, the entry angle of the shovel tip determines both the contact area with the soil and the cutting force. When the entry angle is moderate, the subsoiler shovel can effectively penetrate the soil while maintaining low resistance, thereby achieving efficient deep loosening operations. Since the shovel wings are subjected to the same forces as the shovel tip, their entry angle likewise has a significant influence on the soil disturbance area. Moreover, because the wings are wider than the tip, shovel wing width also strongly affects the disturbance area. Therefore, selecting an appropriate shovel tip entry angle, shovel wing inclination, and wing width is critical to optimizing subsoiler shovel performance. The optimal parameters will be determined through subsequent simulation experiments.

According to the mechanical contact model between the soil and the shovel handle, an arc-shaped shovel handle reduces the push-cut angle between the soil particle mass point and the shovel handle compared to a vertical shovel handle. This reduction in the push-cut angle effectively lowers ploughing resistance and mitigates stress concentration, helping to prevent shovel handle failure. Additionally, in contrast to traditional straight designs, the arc-shaped shovel handle better conforms to the natural flow of soil, reducing resistance during soil entry and facilitating smoother soil movement during subsoiling operations. The shovel handle width is most effective when the ratio of the shovel handle width to the shovel tip length is between 0.68 and 1.04. Therefore, based on a shovel tip length of 160 mm and the optimal ratio range, the shovel handle width is calculated to be 110 mm. As noted in the literature (*Chen et al., 2021*), shovel handle thickness also affects tillage resistance. Excessive thickness increases traction resistance, while insufficient thickness reduces the soil-crushing effect and increases the risk of structural failure. Referring to the JB/T 9788–2020 "*Subsoiler Shovel and Subsoiler Shovel Handle"* standard, the shovel handle thickness is set to 18 mm. The height of the shovel handle depends on the subsoiling depth, and for the target working depth, it is calculated to be 380 mm.

Discrete element simulation experiment for subsoiling operation

Operational modelling

Soil parameter determination was conducted using samples from the black soil region of Northeast China to obtain accurate soil characteristic values. Based on these measured parameters, a soil particle model was established. Pre-tests showed that enlarging the particle diameter by a factor of 1 to 10 had no significant impact on the simulation results, allowing the model to be simplified accordingly. To more accurately simulate real soil behaviour, the Hertz-Mindlin with JKR contact model was selected, as it effectively captures soil cohesion and bonding phenomena (*Zang et al., 2022*). A soil trench was created in EDEM 2022, and a particle factory was used to populate the trench with a bed of soil particles.

To ensure efficient and accurate simulation, the full machine model was simplified by retaining only the subsoiler shovel for analysis. This reduction in model complexity significantly decreased computational load, enabling more efficient simulations (*Wang et al., 2017*). The subsoiler shovel model, created in SolidWorks 2023, was exported in *.slt* format and imported into EDEM 2022 software. The material of the subsoiler shovel was defined as 65-gauge steel, with a density of 7850 kg/m^3, a Poisson's ratio of 0.3, and a shear modulus of 7.8×10^{10} Pa.

The established soil particle model and subsoiler shovel model were imported into EDEM 2022 software. Contact parameters between soil particles, as well as between soil particles and the subsoiler shovel, were defined based on relevant literature (*Wang et al., 2017*) and parameters obtained from physical testing. This setup resulted in the subsoiling operation model shown in Fig. 5. The specific simulation parameters are listed in Table 1.

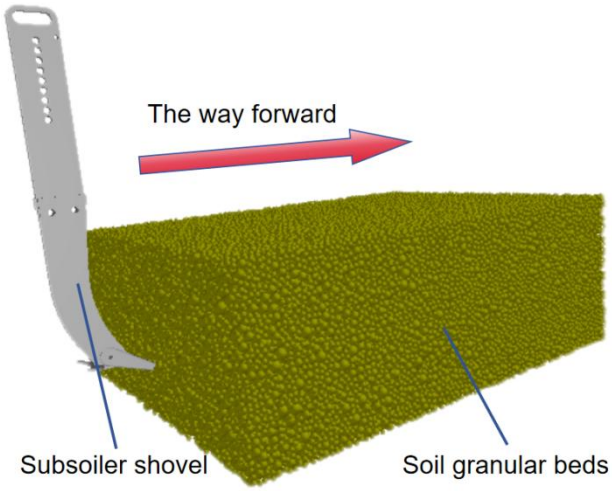

Fig. 5 – Modelling of subsoiling operations

Table 1

Simulation test parameters

Parameter class	Numerical value	Parameter class	Numerical value
Poisson's ratio of soil particles	0.30	Particle-65 steel dynamic friction	0.15
Soil particle density (kg/m^3)	1600	Poisson's ratio of 65 steel	0.35
Soil particle shear modulus (Pa)	1×107	Density of 65 steel (kg/m^3)	7850
Particle-particle coefficient of recovery	0.3	Sear modulus of 65 steel (Pa)	7.8×1010
Particle-particle static friction coefficient	0.7	Soil particle bed thickness (mm)	450
Particle-particle kinetic friction	0.2	Subsoiler shovel horizontal speed (m/s)	1.5
Particle-65 steel restitution coefficient	0.35	Subsoiling depth (mm)	320
Particle-65 steel static friction	0.6	Grid size (mm)	24

Simulation process analysis

After configuring the parameters of the subsoiling operation model, the subsoiling simulation was conducted. Upon completion, soil disturbance was evaluated by dissecting the soil trench using the post-processing module in EDEM 2022. Transverse cross-sections of the soil disturbance at multiple time points during the subsoiling process are shown in Fig. 6.

In the simulation, particle velocity is represented by colour: red particles indicate the highest velocities, followed by green, and then blue, which represent progressively lower speeds. The variation in particle velocity arises from differences in acceleration caused by contact with the subsoiler shovel. Particles in direct contact with the shovel experience greater acceleration, while the acceleration - and thus the particle velocity - gradually decreases with increasing distance from the shovel.

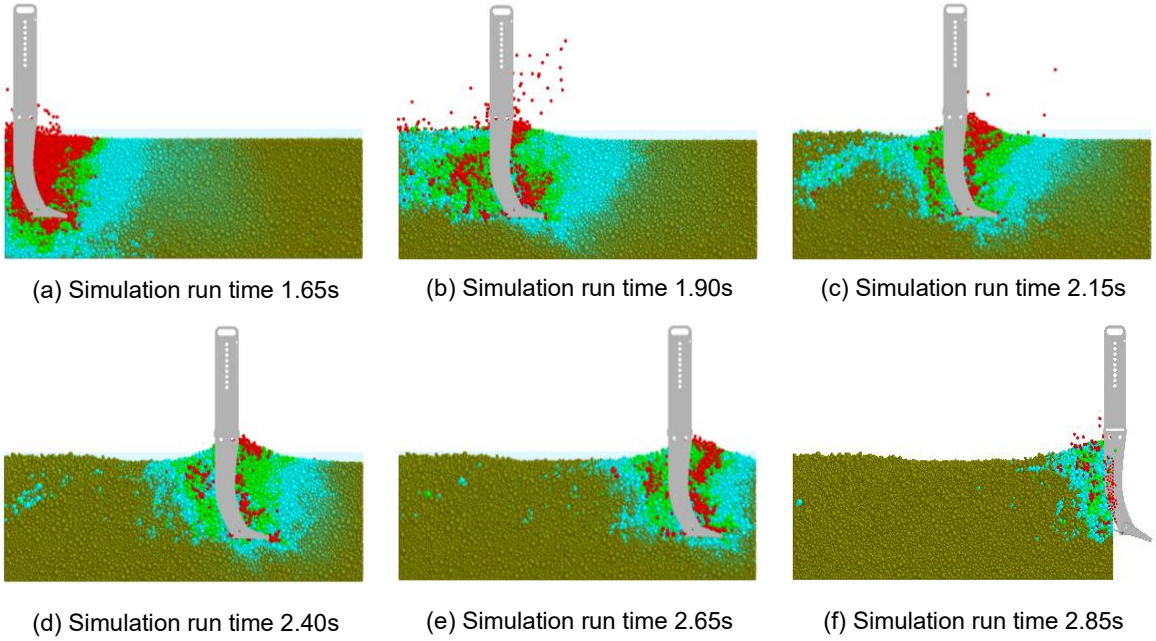

(a) Simulation run time 1.65s (b) Simulation run time 1.90s (c) Simulation run time 2.15s

(d) Simulation run time 2.40s (e) Simulation run time 2.65s (f) Simulation run time 2.85s

Fig. 6 – Transverse section of subsoiling operation

As shown in Fig. 6, when the subsoiler shovel enters the soil particle bed, it undergoes a brief period of instability. This initial disturbance occurs during the early stage of soil contact but dissipates as the shovel continues to move forward. Upon reaching the right side of the soil trench, localized soil particle extrusion is observed. The simulation results indicate that a stable operational phase occurs between 1.90 s and 2.60 s of simulation time.

To accurately evaluate the performance of the subsoiler shovel, it is also necessary to analyse its resistance during operation. Using the post-processing function of EDEM 2022, ploughing resistance data were extracted at different time points. The resulting resistance trend is illustrated in Fig. 7.

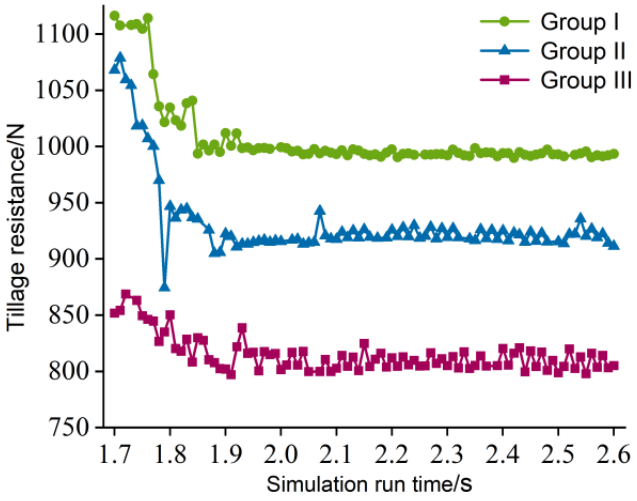

Fig. 7 – Comparison of ploughing resistance in three groups

As shown in Fig. 7, the ploughing resistance is more stable during the simulation time interval from 1.90 s to 2.50 s.

Simulation test design

The mechanical contact model between the subsoiler shovel and soil established earlier identified the primary factors influencing the soil disturbance area. These key factors include the shovel tip entry angle, the inclination angle of the shovel wings, and the width of the shovel wings. To assess their effects on the soil disturbance area Y_1, a multifactor interaction test was conducted. Based on mechanical analysis and pre-tests, the following parameter ranges were selected: shovel tip entry angle X_1 (5°~25°), shovel wing inclination angle X_2 (10°~30°), and shovel wing width X_3 (100mm~120mm). The objective of this test is to determine the optimal structural parameters of the subsoiler shovel under a fixed operational speed; therefore, operating speed was not considered a variable. Based on field conditions and operational experience, the working speed was set to 5 km/h.

A coding table for the test factors was established and is presented in Table 2.

Table 2

Test factor code

Coding	Factor		
	Shovel tip entry angle X_1 (º)	Inclination of shovel wings X_2 (º)	Width of shovel wings X_3 (mm)
1.682	25	30	120
1	21	26	116
0	15	20	110
-1	9	14	104
-1.682	5	10	100

RESULTS AND DISCUSSIONS

Discrete element simulation test results

A multifactor optimization simulation experiment was designed using a quadratic orthogonal rotational combination design. The simulation tests were conducted accordingly, and the evaluation index - soil disturbance area - was measured and recorded at the end of each simulation. The specific test design and corresponding results are presented in Table 3.

Table 3

Pilot programme and results

Number	Factor			Area of soil disturbance Y_1/cm^2
	X_1	X_2	X_3	
1	-1	-1	-1	1645.42
2	1	-1	-1	1305.03
3	-1	1	-1	1516.34
4	1	1	-1	1523.24
5	-1	-1	1	1458.9
6	1	-1	1	1379.36
7	-1	1	1	1405.14
8	1	1	1	1689.5
9	-1.682	0	0	1552.17
10	1.682	0	0	1496.53
11	0	-1.682	0	1400.11
12	0	1.682	0	1551.65
13	0	0	-1.682	1543.28
14	0	0	1.682	1510.96
15	0	0	0	1564.28
16	0	0	0	1574.31
17	0	0	0	1572.44
18	0	0	0	1562.96
19	0	0	0	1550.17
20	0	0	0	1570.56
21	0	0	0	1556.49

Number	Factor			Area of soil disturbance Y_1/cm^2
	X_1	X_2	X_3	
22	0	0	0	1553.63
23	0	0	0	1567.35

Analysis of test results

Regression analysis and analysis of variance (ANOVA) were conducted on the experimental data from Table 3 using Design-Expert 13.0 software. A significance test was applied to identify the most influential factors. Regression equations describing the relationships between the multiple factors and both soil disturbance area and tillage resistance were established. The detailed results of the statistical analysis are presented in Table 4.

Table 4

Analysis of variance for regression modelling of soil disturbance area

Norm	Source of variance	Sum of squares	Degree of freedom	F	P	Significance
Area of soil disturbance Y_1	Model	160896.97	9	57.43	<	**
	X_1	3616.71	1	33.20	<	**
	X_2	26392.81	1	242.31	<	**
	X_3	910.09	1	8.36	0.0123	*
	X_1X_2	63223.90	1	580.46	<	**
	X_1X_3	36222.21	1	332.56	<	**
	X_2X_3	3496.57	1	32.10	<	**
	X_1^2	4630.84	1	42.52	<	**
	X_2^2	18594.01	1	170.71	<	**
	X_3^2	4114.77	1	37.78	<	**
	Residual	1415.96	13			
	Lack of fit	829.42	5	2.26	0.1458	
	Error	586.54	8			
	Sum total	162312.93	22			

As can be seen from Table 4, the regression model P-values are less than 0.01, indicating that the models are all highly significant. In the regression model of soil disturbance area, X_1, X_2, X_1X_2, X_1X_3, X_2X_3, X_1^2, X_2^2, X_3^2 have a highly significant effect on the soil disturbance area, and X_3 has a significant effect on the soil disturbance area. Based on these results, a regression equation relating the factors to soil disturbance area was established.

$$\begin{aligned} Y_1 = {} & 1563.91 - 16.27X_1 + 43.96X_2 - 8.16X_3 \\ & + 88.90X_1X_2 + 67.29X_1X_3 + 20.91X_2X_3 \\ & - 17.07X_1^2 - 34.21X_2^2 - 16.09X_3^2 \end{aligned} \quad (15)$$

To facilitate visual analysis of the relationships between the influencing factors and the evaluation index, response surface plots were generated using Design-Expert 13.0 software. The resulting response surfaces are shown in Fig. 8.

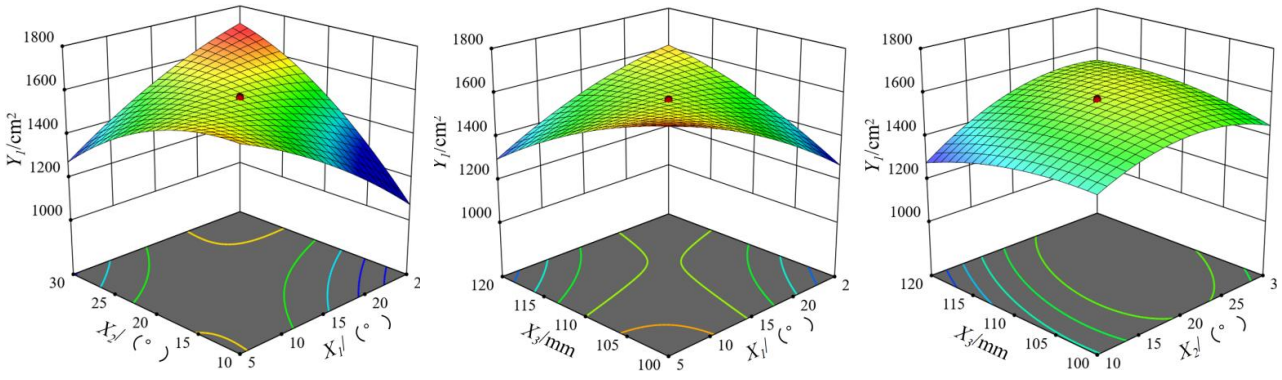

(a) (b) (c)

Fig. 8 – Response surface plots between factors and area of soil disturbance

As can be seen from Fig. 8(a), with the gradual increase of shovel tip entry angle and shovel wing inclination angle, the soil disturbance area shows a trend of small decrease and then large increase. When the shovel tip entry angle changes, the soil disturbance area change interval is larger, so the effect of the shovel tip entry angle on the soil disturbance area is more significant compared to the shovel wings inclination angle. As can be seen from Fig. 8(b), with the gradual increase of shovel tip entry angle and shovel wing width, the soil disturbance area shows a trend of large decrease and then small increase. When the shovel tip entry angle varies, the variation interval of soil disturbance area is larger, so the effect of shovel tip entry angle on soil disturbance area is more significant compared with shovel wings width. From Fig. 8(c), it can be seen that as the shovel wings inclination angle and shovel wings width gradually increase, the soil disturbance area appears to increase firstly and then tends to flatten the change trend. When the shovel wings inclination angle and shovel wings width change, the change interval of soil disturbance area is basically the same, so the influence of shovel wings inclination angle and shovel wings width on soil disturbance area is basically the same.

To determine the optimal combination of influencing factors, an optimization design was carried out. A parametric mathematical model was established based on the boundary conditions of the test factors. Following the objective of maximizing the soil disturbance area, a nonlinear programming model was constructed:

$$\begin{cases} \max Y_1 = (X_1, X_2, X_3) \\ s.t. \begin{cases} 5 < X_1 < 25 \\ 10 < X_2 < 30 \\ 100 < X_3 < 120 \end{cases} \end{cases} \quad (16)$$

The multi-objective optimization module in Design-Expert 13.0 was used to optimize the parameter combinations. Through this process, the optimal structural parameters for the subsoiler shovel were obtained. Based on the optimisation results, a reasonable combination of parameters was selected. When the shovel tip entry angle X_1 is 20.68°, the shovel wing inclination angle X_2 is 27.54°, and the shovel wing width X_3 is 103.72 mm, the soil disturbance area $Y_1$is optimal reaching 1699.80 cm^2. After the optimisation results, in order to facilitate the post-processing, the shovel tip entry angle X_1 is taken as 21°, the shovel wing inclination angle X_2 as 28°, and the shovel wing width X_3 as 104 mm. The optimised parameters are simulated and the soil disturbance area Y_1 is 1690.34cm^2, which is basically consistent with the optimised results.

Benchtop validation experiments

To validate the optimal parameter combination of the subsoiler shovel obtained from the discrete element simulation, a benchtop testing apparatus was developed. The test bench includes components such as a connecting arm, drive motor, single-axis lifting mechanism, guide rail, soil tank, control system, and travelling wheels. The soil tank was pre-filled with representative black soil from Northeast China to replicate actual field conditions. The structural layout of the strip minimum tillage subsoiling and fertilizing test bench is shown in Fig. 9(a).

(a) Structural diagram of the pedestal

1.Travelling wheel; 2 Drive motor; 3.Soil tank; 4.Strip minimum tillage subsoiling fertilizer applicator; 5.Single-axis lifting mechanism; 6.Connecting arm; 7.Guide rail

(b) Actual working conditions of subsoiler shovel in the tillage layer

1. Soil; 2. Shovel handle; 3. Shovel wings; 4. Shovel tip

Fig. 9 – Structural layout of the benchtop platform and working conditions of the subsoiler shovel

Based on the optimal working parameters for the subsoiler shovel obtained from the simulation tests, a winged subsoiler shovel was fabricated. Since the optimized parameters included decimal values, they were rounded for ease of manufacturing: the entry angle was set to 21°, the shovel wing inclination to 28°, and the shovel wing width to 104 mm. The manufactured subsoiler shovel was then mounted on the strip minimum tillage deep loosening fertilization machine. The fertilization machine was connected to the mounting arm, and the insertion depth of the subsoiler shovel into the soil was adjusted accordingly. To observe the in-soil behaviour of the subsoiler shovel, the surrounding soil was cleared after placement. The working condition of the shovel in the tillage layer is shown in Fig. 9(b).

To measure the actual soil disturbance area, it was necessary to extract the disturbed furrow profile after testing. A point within the stable velocity phase was selected as the furrow extraction location. The soil in front of this point was excavated to create a vertical cross-section perpendicular to the trench bottom. The disturbed soil was then carefully cleaned to expose the complete furrow profile. A flexible marker tape was positioned along the trench wall to delineate the profile, and imaging equipment was placed horizontally in front of the exposed cross-section to capture a clear image of the disturbance pattern. The captured image was imported into MATLAB 2020b to extract coordinate data representing the soil disturbance contour, as shown in Fig. 10(a) and (b). These coordinates were then imported into ORIGIN 2021 software to reconstruct the furrow profile and calculate the corresponding soil disturbance area. The final disturbance pattern is illustrated in Fig. 10(c).

(a) Original image (b) Extraction of furrow images (c) ORIGIN maps soil disturbance furrow patterns

Fig. 10 – Flowchart for obtaining area of soil disturbance

Three bench tests were conducted on 3 April 2025, with the soil surface levelled after each trial to ensure consistent initial conditions. Following each test, the soil disturbance area was calculated using ORIGIN2021 software. The disturbance areas recorded for the three trials were 1653.67cm^2, 1665.23cm^2, and 1649.35cm^2, respectively, yielding an average value of 1666.08cm^2. It should be noted that while the discrete element simulation assumed uniform soil particle density and compaction, the actual test conditions introduced variability. In practice, the soil density was not completely uniform across the test plots, and the presence of soil clods introduced inconsistencies in compaction. These factors contributed to the discrepancy between the simulated and measured results. The difference between the average actual disturbance area and the simulated result was -34.26cm^2, which falls within an acceptable error range.

CONCLUSIONS

(1) Based on the prevalent soil compaction issues in the black soil region of Northeast China and the requirements of the strip minimum-tillage cropping pattern, a novel winged subsoiler shovel was designed. This design enhances soil disturbance and effectively addresses existing soil structure problems while maintaining compatibility with strip-tillage operations.

(2) A mechanical contact model between the subsoiler shovel and soil was established to analyse the operational forces acting on the shovel. Key design parameters influencing subsoiling quality were identified through this model.

(3) A discrete element method (DEM) simulation was conducted to model subsoiling operations. An orthogonal experimental design was implemented using the shovel tip angle, wing inclination angle, and wing width as test factors, with the soil disturbance area as the primary evaluation index. Based on the simulation results and response surface optimization, the optimal structural parameters of the subsoiler shovel were determined. A bench-scale validation test confirmed the effectiveness of the optimized design, with the average actual soil disturbance area measured at 1666.08 cm², closely aligning with the simulation results and meeting the operational requirements for minimum tillage subsoiling.

ACKNOWLEDGEMENT

This paper was supported by the National Key Research and Development Programme of China (2023YFD1501005-06) and the Heilongjiang Provincial Key Research and Development Programme (2022ZX05B05-01).

REFERENCES

[1] Chen J., Liang X., Qi G., Zhang Y., Wang S., & Xing S. (2021). Optimization of mechanical structure of soil subsoiling and operation test (土壤深松机械结构优化及作业试验) [J]. *Tianjin Agriculture and Forestry Science and Technology*, Issue 4, pp. 8-10.

[2] Gao Z., Lu C., Wei X., Li H., He J., & Wei Q. (2023). Design and Experiment of Co-stirring Combined Corn Strip-Straw Cleaning Device (协拨组合式玉米条带秸秆清理装置设计与试验) [J]. *Transactions of the Chinese Society for Agricultural Machinery*, Vol. 54, Issue 10, pp. 68-79.

[3] Li B., Chen Y., & Chen J. (2018). Comparison of Two Subsoiler Designs Using the Discrete Element Method (DEM). *Transactions of the ASABE*, Vol. 61, Issue 5, pp. 1529-1537.

[4] Manuwa, S I. (2009). Performance evaluation of tillage tines operating under different depths in a sandy clay loam soil. *Soil & Tillage Research*, Vol. 103, Issue 2, pp. 399-405.

[5] Ma C. (2022). Design and experiment of deep fertilization strip tillage device for corn in Northeast China (东北玉米区深施肥带状耕作装置设计与试验). *Chinese Academy of Agricultural Mechanization Sciences*.

[6] Wang Q., Cao X., Wang C., Li H., He J., Lu C. (2021). Research Progress of No/Minimum Tillage Corn Seeding Technology and Machine in Northeast Black Land of China (东北黑土地玉米免少耕播种技术与机具研究进展) [J]. *Transactions of the Chinese Society for Agricultural Machinery*, Vol. 52, Issue 10, pp.1-15.

[7] Wang J., Tang H., Wang J., Huang H., Lin N., Zhao Y. (2017). Numerical Analysis and Performance Optimization Experiment on Hanging Unilateral Ridger for Paddy Field (悬挂式水田单侧修筑埂机数值模拟分析与性能优化) [J]. *Transactions of the Chinese Society for Agricultural Machinery*, Vol. 48, Issue 8, pp. 72-80.

[8] Zhang Z., Yin Z., Yu P., Qi Z., Wei Y., Li A. (2024). Effects of Soil and Water Conservation Measures on Soil Physical and Chemical Properties in Slope Farmland in Black Soil Region (黑土区坡耕地水土保持耕作措施对土壤理化性状的影响) [J]. *Transactions of the Chinese Society for Agricultural Machinery*, Vol. 55, Issue 1, pp.282-293.

[9] Zhao S., Wang J., Chen J., Yang Y., & Tan H. (2018). Design and Experiment of Fitting Curve Subsoiler of Conservation Tillage (保护性耕作拟合曲线型深松铲设计与试验) [J]. *Transactions of the Chinese Society for Agricultural Machinery*, Vol. 49, Issue 2, pp. 82-92.

[10] Zheng K., He J., Li H., Diao P., Wang Q., & Zhao H. (2016). Research on Polyline Soil-breaking Blade Subsoiler Based on Subsoiling Soil Model Using Discrete Element Method (基于离散元深松土壤模型的折线破土刃深松铲研究) [J]. *Transactions of the Chinese Society for Agricultural Machinery*, Vol. 47, Issue 9, pp. 62-72.

[11] Zhang L. (2013). Study on Resistance Reduction Technology of Subsoilers (深松铲减阻技术). *Jilin University.*

[12] Zhou Y. (2006). Force Mathematical model and computer simulation of subsoiling (深松铲受力数学模型与计算机模拟). *Henan Agricultural University.*

[13] Zhang X., You Y., Wang D., Wang Z., Liao Y., Lv J. (2022). Design and Experiment of Soil-breaking and Root-cutting Cutter Based on Discrete Element Method (基于离散元法的板结草地破土切根刀优化设计与试验) [J]. *Transactions of the Chinese Society for Agricultural Machinery*, Vol. 53, Issue 11, pp.176-187.